RSC Advances

ROYAL SOCIETY OF CHEMISTRY

www.rsc.org/advances

A comparative study on the efficacy of different probes to predict the photo-activity of nano-titanium dioxide toward biomolecules

A. Marucco,[a] E. Carella[a] and I. Fenoglio[a*]

[a] *Dip. Chimica, ''G. Scansetti'' Interdepartmental Centre for Studies on Asbestos and other Toxic Particulates, and NIS – Nanostructured Interfaces and Surfaces, University of Torino, Italy.*

** corresponding author. ivana.fenoglio@unito.it. Phone +39 11 6707506.*

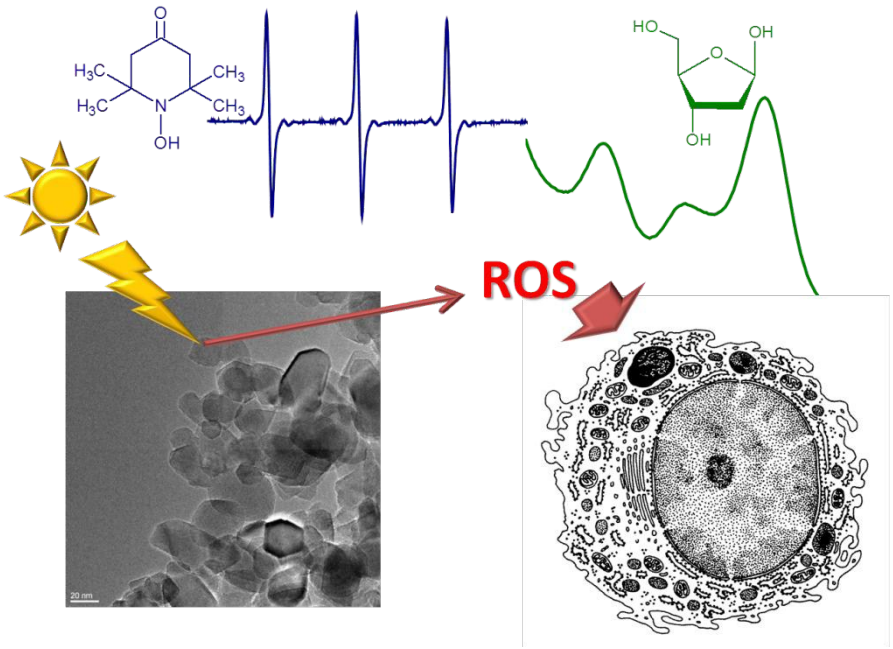

A systematic study has been performed to select cell-free tests able to predict the photo-activity of nano-TiO_2 in living organisms.

Abstract

TiO_2 is a reactive material being able to cause the degradation of organic molecules following activation by UV light. This reactivity may be useful, e.g in environmental or medical applications, but undesired when TiO_2 is used as UV filter in cosmetics and composites since it reduces the photo-stability of the material, and represents a possible pathway of injury. Conventional methods to measure the photo-activity of TiO_2 include the degradation of small molecules or dyes. However the suitability of these methods to predict the photo-activity of TiO_2 in biological systems is uncertain. This is the first product of a study, conducted within the FP7 EU project SETNanoMetro, that has as main goal the standardizations of protocols to assess the oxidative potential of TiO_2 nanopowders in biofluids. Here, the ability of a series of nano-TiO_2 powders exibiting different crystalline phases to degrade rhodamine B, a dye commonly used in photo-catalysis, and two model biomolecules (linoleic acid and 2-deoxyribose) under simulated sunlight was compared. Electron paramagnetic resonance (EPR) spectroscopy associated to different spin-probes or spin-traps was used to elucidate the reactive species involved in the processes. The results show how the photo-efficiency of TiO_2 is affected by the kind of probe and by the presence of species that adsorb at the surface of the nanoparticles underlining the need of appropriate standard operating procedures (SOP) to evaluate the oxidative damage potential of semiconducting nanomaterials.

1. Introduction

Nanotechnology industry is expanding at a rapid rate in the last years. Among the manufactured nanomaterials, titanium dioxide is one of the most widely used. The amount of TiO_2 produced every year worldwide is estimated to be between 1000-10 000 tons.[1,2] Micrometric TiO_2 powders are commonly used as white pigment in paint, cosmetics, food and as filler in rubber, plastics and cement. The usage of titanium dioxide as pigment is due to its high reflective index that allows particles to refract the visible light. On the contrary, nanometric titanium dioxide, being transparent to visible light but opaque to ultraviolet light, is extensively employed as UV blockers in sunscreens and plastics.[3,4] TiO_2 is also a well-known photo-catalyst. When illuminated with UV light it generates high amount of reactive species that efficiently degrade organic molecules. For this reason it gains significant interest in polluted water and air remediation,[5] in the production of self-cleaning coatings and textiles[6] and, more recently, as photo-sensitizer in the photodynamic therapy of cancer (PDT)[7] and bacterial infections.[8] When titania absorbs photons with energies higher or equal to its band gap (>3.2 eV for anatase), electrons are excited in the conduction band (e^-_{CV}) leading to the formation of a positive hole in the valence band (h^+_{VB}). These charge carriers can recombine each other or migrate at the surface and react with electron donors or acceptors.[9] For example, photo-generated electrons may reduce oxygen to superoxide radicals ($O_2^{\bullet-}$) (equation 1) while photo-generated holes oxidize water leading to the generation of the highly reactive hydroxyl radicals ($OH^\bullet$) (equation 2).

$$O_2 + e^-_{cv} \rightarrow O_2^{\bullet-} \quad (1)$$

$$HO^- + h^+ \rightarrow HO^\bullet \quad (2)$$

Hydroxyl and superoxide radicals are therefore among the primary reactive species that are formed. However, they may further react to give secondary species that are hydroperoxyl radicals (·OOH), the conjugate acid of the superoxide anion (equation 3), and hydrogen peroxide (H_2O_2), the one-electro reduction product of superoxide anion (equation 4). Hydrogen peroxide may further react with conduction band electrons generating hydroxyl radicals (equation 5).

$$O_2^{\bullet-} + H_2O \leftrightarrows HO_2^\bullet + H^+ \quad pKa = 4.7 \quad (3)$$

$$O_2^{\bullet-} + e^-_{CV} + 2H^+ \rightarrow H_2O_2 \quad (4)$$

$H_2O_2 + e^-_{CV} \rightarrow HO^{\bullet} + HO^-$ (5)

Singlet oxygen ($^1O_2$) is also a primary reactive specie. The mechanism of generation is still under debate and different pathways has been suggested.[10, 11]

Titanium oxide is commercially available in several different forms differing for crystalline phase (anatase and rutile are the most common), particle size and bulk or surface modifications. All this forms have different photo-activity. Crystalline phase and size are known to modulate the photo-catalytic efficiency due to differences in band gap values or in rate of recombination of the charge carriers.[9, 12] Coatings may decrease the photo-reactivity (e.g. in cosmetic applications) while doping with various elements is generally applied to increase the photo-efficiency of TiO_2 in particular in the visible region.[13]

The photo-efficiency of TiO_2 is commonly evaluated by measuring the ability of the powder to degrade small organic molecules (e.g. methanol) or organic dyes (e.g. metylene blue or rhodamine B). These methods are suitable to identify the best candidates in industrial applications where TiO_2 react in the gas-phase or solutions having simple composition, e.g. in the manufacture of self-cleaning coatings. However they may be not predictive of the reactivity of TiO_2 in complex environments like those encountered in cells, extracellular matrixes and cell media. Biofluids, in fact, contains several molecules that may adsorb and modify the photo-efficiency of TiO_2. Furthermore, a specificity of the ability of TiO_2 to react with biomolecules exists, due to differences in diffusion rate of molecules from bulk solution to the surface[14] and in the tendency to adsorb at the surface. A deep knowledge of the chemistry that govern such complex processes may help in assessing tools for the prediction of the oxidative potential of the various TiO_2 forms in living systems.

Here, a commercial sample of TiO_2 (Aeroxide P25) known for its high photo-reactivity,[15] a homemade sample of anatase/rutile mixed phase titania, one sample of anatase, and two samples of commercial rutile (one coated) have been tested for the their ability to degrade two model biomolecules, linoleic acid and 2-deoxyribose under visible light irradiation. This reactivity has been compared with those toward rhodamine B.[6] EPR spectroscopy associated to different spin trapping agents and probes has been used to identify and quantify the primary ROS generated to gain information on the mechanisms of reaction.

2. Results

2.1 Physicochemical characterisation of TiO_2 samples

The samples used in this work were chosen because of the high degree of purity, thus avoiding any effect due to impurities, and because similar in primary particle size and surface area but different regarding crystalline phases (Table 1).

The X-ray diffraction (XRD) patterns of T-A/R and T-A/R P25 reveal the presence of very sharp peaks corresponding to anatase and rutile phases in similar proportion (Table 1, SI) in both samples. However T-A/R exhibited a specific surface area lower than the commercial sample P25 that corresponds to a higher particles size (Figure 1A,B). Well-defined crystallographic planes are visible in the transmission electron microscopy (TEM) images (Figure 1A,B, insets), confirming the high degree of crystallinity of the materials.

The XRD diffractogram of the nanometric anatase sample (T-A) exhibited a broadening of the diffraction peaks (SI), revealing a highly disordered structure which was a direct consequence of the small size of primary particles as shown by the TEM images (Figure 1C). All samples appear organized in aggregates with a wide distribution of size.

The crystalline phase of the commercial rutile specimens (T-R1,2) was confirmed by means of XRD. T-R1, as suggested by the specific surface area (SSA) and the TEM images, was characterized by nanometric spherical particles with a percentage of rod particles (Figure 1D). The sample T-R2 contains a 1-5 % of silicon and aluminium suggesting the presence of a coating (Table 1).

The samples have been also characterized in aqueous suspension by measuring their ζ potential (Table 1 and SI). Being TiO_2 an amphiphilic substance, the surface of particles may be in water both positive or negative depending upon the pH. At pH 7.4, the ζ potential was negative and similar for all powders except for T-A/R P25 that showed a slightly lower value. All samples reached a point of zero charge (PZC) at acidic pH. However, the PZC values were significantly different among samples suggesting a different abundance of charges at the surface in the different specimens. In the case of T-R2 an acidic PZC was expected due to the presence of silica and alumina.

2.2 Degradation of linoleic acid and 2-deoxyribose

The oxidative potential of the powders was evaluated by measuring the ability to degrade two models molecules, linoleic acid, an unsaturated fatty acid abundant in cell

membranes, and 2-deoxy-ribose, fundamental component of the DNA double helix. The degradation was evaluated by measuring the amount of malonyldialdehyde (MDA), the major degradation product of unsaturated fatty acids[16] and 2-deoxy-ribose, formed.

The results, expressed as absorbance at 535 nm correspondent to the coloured adduct of thiobarbituric (TBA) with MDA, are reported in Figure 2, while the spectra are reported in the supplementary information. T-A/R, T- A/R P25 and T-A showed a marked activity toward linoleic acid, while the other specimens did not induce the degradation of the molecule. A similar order of reactivity was found in the case of 2-deoxyribose degradation, however, in this test T-R1 was active albeit at less extent than the anatase containing samples.

Note that in both reactions, the presence of picks in the wavelengths range 430-510 nm (SI) suggests the formation of degradation products other than MDA.

2.3 Degradation of rhodamine B

A different trend was observed in the case of rhodamine B degradation. All samples, except T-R2, rapidly decrease of the absorbance at 555 nm (Figure 3). The solution gradually turned form purple to green and a new pick at 498 nm appeared (SI, S4). This pick corresponds to the maximum of absorbance of the de-ethylated product rhodamine (reaction 6).[17]

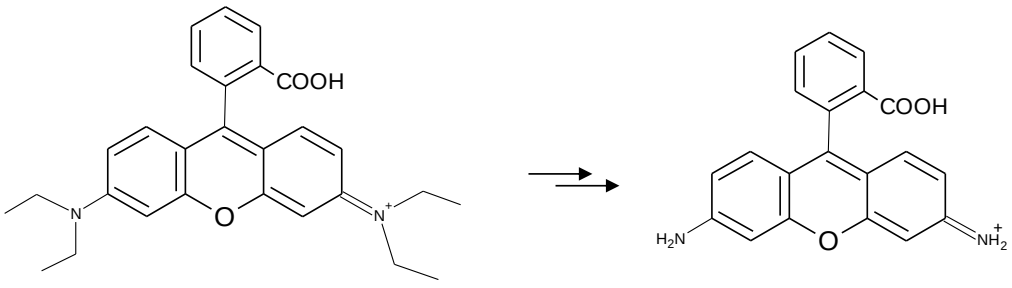

rhodamine B rhodamine (6)

In the case of T-A/R and T-A a decrease of the pick intensity at 498 nm was observed after 90 minutes suggesting that for, these samples, an additional degradation of rhodamine occurs (SI).

2.4 Generation of hydroxyl radicals and oxidative reactivity

The amount of hydroxyl radicals generated following reaction (2) was measured by electron paramagnetic resonance (EPR)-spin trapping technique. Hydroxyl radicals were detected by trapping them with the spin trap 5,5-dimethyl-1-pyrroline-N-oxide

(DMPO) in phosphate buffer at neutral pH (Figure 4A). Buffer is used to maintain the pH at a near neutral value thus avoiding any effect due to pH variation and to simulate the physiological pH and osmolarity.

A typical 1:2:2:1 signal of the adduct DMPO-HO$^{\bullet}$ was observed by EPR for anatase and for the two mixed phase samples after 60 minutes of irradiation with simulated solar light. Oppositely, no signal was detected with the two rutile powders. The intensity of the signal obtained with anatase was the highest followed by the T-A/R, whereas T-A/R P25 showed the lowest intensity. The intensity of the EPR signals obtained in the present conditions was however very low. This is not due to an instability of the [DMPO-OH]· adduct or to a low kinetic of formation, both known to be relatively high,[18, 19] but to the low amount of [DMPO-OH]· generated in this conditions. On the other hand DMPO is poorly selective toward hydroxyl radicals generated by TiO_2 since it was reported to reacts also with superoxide radicals,[20] singlet oxygen[21] and the TiO_2 surface[22] giving several degradation products.

Alternatively, formic acid may be added to the reaction. In this case, the overall oxidative capacity of TiO_2 is evaluated since this molecule, is able to reacts both with hydroxyl radicals (reaction 8) and vacancies (reaction 9) giving carbon-centred radicals ($^{\bullet}CO_2^-$) that form with DMPO a very stable product. [19, 23]

$$HCOO^- + HO^{\bullet} \rightarrow {}^{\bullet}COO^- + H^+ \quad (8)$$

$$HCOO^- + h^+ \rightarrow {}^{\bullet}COO^- + H^+ \quad (9)$$

As expected an intense EPR signal correspondent to the adduct DMPO-COO$^{\bullet-}$, was observed for all samples except R2 (Figure 5). The anatase and the two mixed phase samples generated high amount of free radicals that increase during time, followed by T-R1, while no signal was detected for the sample T-R2.

2.5 Generation of superoxide anion radicals

The primary radical species generated in water by photo-generated electrons is the superoxide anion (reaction 1). This specie may remain adsorbed at the surface or it may be released in solution. While it may be easily detected by EPR spectroscopy on the dry powder[23] or in organic solvents,[24] the detection of this species in water is not trivial. This may be due to both the lower solubility of oxygen in water by respect to organic

solvents, or to the occurrence, in water, of the competitive dismutation of superoxide radicals to oxygen and hydrogen peroxide (reaction 10):

$$2O_2^{-\cdot} + 2H^+ \rightarrow O_2 + H_2O_2 \qquad (10)$$

Here we use N-tert-butyl-α-phenylnitrone (PBN) as spin trap, and performed the reactions in cyclohexane (Figure 4B). The PBN/$O_2^{-\cdot}$ adduct is in fact very unstable in water, while has a longer half-life in organic solvents.[25] The typical signal of the PBN/$O_2^{-\cdot}$ adduct was observed for all samples except TiO_2-R2. The highest signal intensity were generated by the mixed phase samples followed by anatase and rutile. The intensity of the signal was in any case low, suggesting that the rate of degradation of the PBN/$O_2^{-\cdot}$ adduct in this condition is too high compared to the rate of formation, leading a poor accumulation of the radical species generated.

Both DMPO and PBN probes appear therefore not suitable to quantify the amount of radical species formed by TiO_2 because of the low intensity of the signals. Nevertheless they are a proof of the effective generation of $HO^{\bullet}$ and $O_2^{-\cdot}$.

2.6 Generation of ROS measured by using TEMPONE-H

Sterically hindered cyclic hydroxylamines have been used in several studies as probe for the presence of ROS in cells.[26] Hydroxylamines may in fact be oxidized to paramagnetic nitroxide radicals that can be detected by EPR (reaction 7). This reaction occurs in the presence of hydroxyl radicals, [27] superoxide radicals[28] and Fe^{3+} or Cu^{2+} ions.[29]

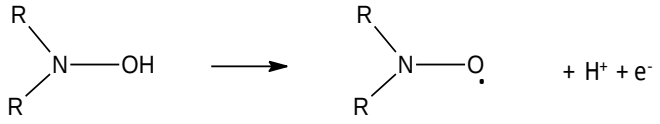

(7)

Here, the hydroxylamine TEMPONE-H has been used to evaluate the reactivity of the various TiO_2 specimens. This molecule produces the highly stable radical TEMPONE[30] that may be easily detected by EPR spectroscopy. Since the radical TEMPONE is very stable we might assume that the intensity of the signal is proportional to the amount of radical species generated. Note however that TEMPONE was reported to catalyze the

dismutation of superoxide in some conditions.[31] Therefore, the amount superoxide generated might be much higher than the amount of radicals detected.

In water, the anatase and the mixed phase samples generate high amount of radicals species (Figure 6A) and the generation was sustained with time. Oppositely, the rutile T-R2 was completely inactive in agreement with the other tests performed.

Similarly to what found with rhodamine B, and differently to what found with sodium formate, linoleic acid and 2-deoxyribose, the sample T-R1 was very reactive toward TEMPONE-H probe. To evaluate if the presence of phosphate buffer, present in the latter three tests but not in the first one, was responsible of such different reactivity the test was also repeated in phosphate buffer (Figure 6B). The reactivity decreased for all samples but more for T-R1 so that the order of reactivity toward TEMPONE-H became similar to that observed with the two biomolecules.

2.7 Generation of singlet oxygen

The generation of this species has been evaluated using the spin probe 4-oxo-TMP that reacts with singlet oxygen leading to the formation of TEMPONE (Figure 7). The reaction was firstly carried out in an organic solvent. In this condition, the typical signal of the radical TEMPO was detected for all samples except the two rutile specimens, being T-A/R the more reactive followed by anatase (Fig. 7A).

The generation of singlet oxygen was further confirmed by using a coloured dienic molecule (rubrene) as probe using a protocol previously reported.[32] Singlet oxygen reacts with the orange rubrene in a Diels–Alder [4 + 2] cycloaddition producing a colourless endoperoxide.[33, 34] The amount of singlet oxygen generated is thus inversely proportional to the absorbance measured from the supernatant of the solution in the 400–600 nm range. In Fig. 7B the spectra of the solution of rubrene irradiated with the simulated solar light in the presence of each TiO_2 sample is compared with the spectra of the solution irradiated in the absence of the powders. The trend of reactivity was similar to those found with the 4-oxo-TMP probe.

The generation of singlet oxygen was also measured in water by using the 4-oxo-TMP probe (Fig. 7C,D). As expected the intensity of the EPR signals was very low. In fact singlet oxygen has a low half-time in water, due to the deactivation of singlet oxygen by energy transfer to the surrounding molecules such as H_2O.[24, 35] Quantification of the amount of molecules generated suggested however that the anatase containing samples was substantially more reactive than rutile.

3. Discussion

The ability of some micro/nanomaterials to generate ROS is recognized as one of the mechanisms of toxicity since an excess of ROS leads to cell damage or death. [36, 37] This property needs therefore to be suppress in designing safe nanomaterials. Recently, a report of the Scientific Committee on Consumer Safety (SCCS) of the European Commission (COLIPA n° S75) recommended not to use TiO_2 with substantially high photo-catalytic activity in sunscreen formulations. In fact, the European legislation does not pose at the moment any limitation to the kind of TiO_2 that can be used of in cosmetics. Photo-activity may be also considered a determinant of eco-toxicity since the generation of ROS may lead to microbes and other organisms death in the environment.[38] On the other hand, photo-activity may be exploited for therapeutic purposes, e.g. in photodynamic therapy of cancer[7] or to fight against bacterial infections.[39] In all these cases TiO_2 acts in complex systems, like extracellular matrixes or biofilms, containing a large variety of molecular and ionic species that may dramatically modify its reactivity.

The availability of tests able to predict the oxidative potential of TiO_2 in such complex systems may help in developing safe nanomaterials.

3.1 The photo-reactivity of TiO_2 depends upon the experimental conditions

Linoleic acid and 2-deoxyribose are two model molecules relevant under a biological point of view: linoleic acid is a good model for unsaturated fatty acids that are commonly present in the cell membranes, while 2-deoxyribose is a constituent of nucleic acids. Both these molecules are known to be degraded by ROS, however the reactivity toward the various radical species is different. The ROS-mediated degradation of unsaturated fatty acids is commonly called lipoperoxidation, and may be initiated by both hydroxyl radicals or singlet oxygen.

In the first case, the abstraction of an allylic hydrogen by hydroxyl radicals leading to the formation of a carbon centred radical is believed to be the starting reaction (reaction 11). Following the reaction with oxygen hydroperoxides are formed (reaction 12) that in turn degrade to aldehydes. Malonyldialdehyde (MDA) is one of the main final products, and therefore it is widely used as marker of lipoperoxidation.[16]

$$\text{-CH=CH-CH}_2\text{-CH=CH-} + R^{\cdot} \rightarrow \text{-CH=CH-CH}^{\cdot}\text{-CH=CH-} \quad (11)$$

$$\text{-CH=CH-CH}^{\cdot}\text{-CH=CH-} + O_2 + RH \rightarrow \text{-CH=CH-CH(OOH)-CH=CH-} + R^{\cdot} \quad (12)$$

The process may also be initiated by singlet oxygen. This molecule reacts with unsaturated fatty acids giving hydro/endoperoxides that degrade giving the same end-product of the first pathway.

2-deoxyribose is also easily degraded by hydroxyl radicals, and for this reason it has been used to probe the generation of hydroxyl radicals in solution.[40] The oxidation of 2-deoxyribose has been reported to play a critical role in oxidative damage of DNA.[41] The main final product of such degradation is, again, MDA.[41] To our knowledge, no data are available on the reactivity of singlet oxygen toward 2-deoxyribose. The tested powders appear to have different oxidative potential, being the two mixed phase specimens the most reactive, followed by anatase and the two rutile specimens. Oppositely, when tested for their ability to degrade rhodamine B, all samples, except for the coated rutile, elicit very similar reactivity. This difference may be explained since rhodamine B are known to act as sensitizer when adsorbed onto TiO_2: when irradiated with visible light rhodamine B is promoted to an exited state that decays by injecting electron to conduction band of TiO_2 thus increasing the efficiency of TiO_2 under visible light. This process is widely studied for solar cells[42] or in photocatalysis.[43]The degradation is therefore dependent to both the efficiency of the dye/semiconductor system and by the propensity of the surface to adsorb the dye.

Carboxylic acids also adsorb at the surface of TiO_2.[44] In this case sensitization is not expected, and the degradation is a function of the intrinsic oxidative reactivity of the material and its tendency to adsorb the molecule. The order of reactivity toward formate resemble those seen for linoleic acid and 2-deoxyribose being T-R1 and T-R2 less reactive than the anatase containing samples. The observed high reactivity of T-R1 toward rhodamine B may be due to the different mechanism of photo-activation leading the reactivity of the samples in the visible region similar. Another possibility is an effect of the phosphate buffer, that was present in all tests except those with rhodamine B. This effect is clearly seen with TEMPONE-H: the presence of the phosphate buffer decreases the reactivity of all samples toward this molecule, however the effect is much more pronounced on T-R1. The inhibitory effect of the phosphate buffer may be ascribed to differences in pH, lower in water than in phosphate buffer (SI), or to the adsorption of phosphate ions to the Lewis acid sites Ti^{4+} exposed at the surface of titania.[45]

The hydroxylamine TEMPONE-H reacts with the both hydroxyl radicals,[46] and superoxide.[28] Furthermore, this molecule reacts with metals high oxidative state like

iron (III) or Cu(II).[29] Therefore, having a very high reduction potential (E°= +2.53V versus SHE),[47] photo-generated holes likely react with TEMPONE-H giving the TEMPONE radical. This probe appear thus suitable to measure both the overall oxidative and reductive activity of TiO_2.

Since the orders of reactivity of the samples toward TEMPONE-H and formate are similar, we may suppose that superoxide itself plays a minor role in the overall reactivity. Note however that oxidative and reductive activity are strictly linked each other. In fact, the scavenging activity of oxygen toward the photo-generated electrons inhibits the recombination of the charge carriers thus enhancing the oxidative reactivity. The amount of TEMPONE formed is one order of magnitude less than the amount of carboxylate radiclas. This should be ascribed to a higher abundance of formate ions in proximity or adsorbed at the surface, likely due to a combination of an higher tendency of formate ions to adsorb at the surface, an higher rate of diffusion, and the higher concentration of formate ions used in the test by respect TEMPONE-H.

Finally, the generation of singlet oxygen, observed only for the anatase containing samples, likely contributes to the high reactivity of the anatase containing samples toward linoleic acid.

3.2 TiO_2 polymorphs responds differently to experimental conditions

The oxidative potential of the various specimens toward the two biomolecules considered appears to be modulated by the crystalline phase. Note that the reactivity has been measured at equal surface area thus eliminating the effect of the surface area extent.

The high reactivity of T-A/R P25 was expected following what reported in the wide literature available on this material. [15, 48, 49] A similar high reactivity was observed for the homemade mixed phase sample despite the method of synthesis was different form P25 (sol-gel and calcination vs spray pyrolysis) suggesting that the coexistence of the two phase is responsible of the enhancement of the reactivity. Note that the high surface reactivity of P25 specimen has been linked to the high toxicity of this samples[50, 51] also if not previously photo-activated.[52] Almost totally inactive in all test was the rutile sample T-R2, suggesting the presence of a coating of silica/allumina. Unexpectedly [51, 53] the uncoated rutile R1 was found highly reactive toward TEMPONE-H in water, similarly to the anatase and mixed phase samples. However, a significant decrease of reactivity was observed in the presence of phosphate, likely due to the adsorption of

phosphate ions at the surface.[45] The sensitivity of rutile to the presence of phosphate may account for the previously reported low reactivity and, possibly, low in vitro toxicity[54, 55] of rutile specimens since these experiments are performed in the presence of phosphate buffer.[51, 53] Note however that other species able to strongly adsorb at the surface of TiO_2, and possibly to modulate its reactivity, are present on cell media and cells (e.g. carboxylic acids and amines), suggesting the need for further investigations.

4. Conclusions

Among the probes tested TEMPONE-H and DMPO in the presence of sodium formate appear the most suitable to predict the oxidative potential of titania nano-powders toward biomolecules. The presence of phosphates dramatically reduces the reactivity of the various specimens at different extent, being rutile the more affected. Overall, the data herein reported suggest caution in extrapolating data by conventional tests for the evaluation of the photo-efficiency of TiO_2 in living organisms, and in comparing data obtained in different conditions.

5. Experimental

5.1 Preparation of TiO_2 samples

The nanometric anatase powder (T-A) was synthesized by sol-gel method as previously described;[54] a commercial nanometric rutile (T-R1) was purchased from LCM Trading (Italy) while a second sample (T-R2) was a kind gift of Dr. Giovanni Baldi, Colorobbia S.p.A., Florence, Italy; The pyrogenic nanometric mixed phase powder Aeroxide P25 (T-A/R P25) was purchased from Degussa-Evonik (Germany); a second nanometric mixed phase powder was obtained from T-A by calcination in air at 973K. Calcination temperature and time was controlled to obtain a sample having a proportion of anatase and rutile similar to T-A/R P25.

All reactants employed in this work were purchased by Sigma-Aldrich (St. Louis, MO) and used without any other purification treatment albeit otherwise specified. All experiments were performed in ultrapure MilliQ water (Millipore, Billerica, MA).

5.2 X-ray Diffraction (XRD)

XRD spectra measurements were performed by means of a diffractometer (PW1830, Philips) using CoKα radiation, in the (20−90) 2θ range, with step width 2θ = 0.05.

Diffraction peaks have been indexed according to the ICDD database (International Centre for Diffraction Data). The spectra have been elaborated (X'pert Highscore 1.0c, PANalytical B.V.) in order to assess the crystalline phase of the different specimens.

5.3 Surface Area Measurements

The surface area of the particles was measured by means of the Brunauer, Emmett, and Teller (BET) method based on N_2 adsorption at 77 K (Micrometrics ASAP 2020).

5.4 Elemental Analysis

The TiO_2 samples were analyzed using an EDAX Eagle III energy dispersive micro-XRF spectrometer equipped with a Rh X-ray tube and a polycapillary exciting a circular area of nominally 30 μm diameter. Data collection occurred at each point for 200 s detector live time, with X-ray tube settings adjusted for 30% dead time. About 1×10^6 Cps were counted per scan. At least 25 points were collected for each sample.

5.5 ζ Potential

The ζ potential was evaluated by means of electrophoretic light scattering (ELS) (Zetasizer Nano-ZS, Malvern Instruments, Worcestershire, U.K.). TiO_2 particles were suspended in ultrapure water and then sonicated for 2 min with a probe sonicator (100 W, 60 kHz, Sonoplus, Bandelin, Berlin, Germany). The ζ potential was measured at different pH (2- 9) by adding 0.1 M HCl or NaOH to the suspension.

5.6 Morphological Characterization

The morphology of the samples was investigated by electron transmission microscopy TEM (JEOL 3010-UHR instrument operating at 300 kV, equipped with a 2k x 2k pixels Gatan US1000 CCD camera). The powders were suspended in water, sonicated to reduce the agglomeration of particles, deposited on a grid, and the solvent evaporated.

5.7 Illumination conditions

Illumination was performed by a 500 W mercury/ xenon lamp (Oriel Instruments) equipped with an IR water filter to avoid the overheating of the suspensions and a 400 nm cut-off filter. Light irradiance, measured with a photo-radiometer (Delta Ohm S. r. L., Padova, Italy) was of 518.5 W/m^2 (1050-400nm, NIR-Vis) and 67.8×10^{-3} W/m^2 (400-315nm, UVA)

5.8 Degradation of linoleic acid and deoxy-D-ribose

The assay is based on the reactivity of malonyldialdehyde (MDA), a colourless end-product of degradation of both molecules, with 2- thiobarbituric acid (TBA) to produce a pink adduct that absorbs at 535 nm.

The amount of TiO_2 powders corresponding to 1.04 m^2 of exposed surface area was suspended in 2 ml of a buffered (sodium phosphate buffer 10 mM, pH 7.4) emulsion of linoleic acid (1 mM) containing the 2.5 % w/w of ethanol or by a buffered (sodium phosphate buffer 10 mM, pH 7.4) solution of deoxy-D-ribose. The mixture was transferred in a quartz vials and irradiated under continuous stirring for 1 h. The peroxidation was stopped by adding 0.1 ml of butyl hydroxyl toluene (BHT, 0.2 % w/w) to the suspension. The powder was then removed by centrifugation and filtration (cellulose acetate filters, pore ø 0.20 μm) and 2 ml of a solution of TBA (0.034 M) containing HCl (0.25 M) and trichloroacetic acid (TCA, 0.92 M) were added to 1 ml of the solution. The resulting mixture was then heated at the temperature of 373 K for 1 h. After cooling in an ice bath, 3 ml of 1-butanol were added to extract the coloured complex. The UV/vis spectra were measured on the organic phase by means of a UV/Vis spectrophotometer (Uvikon, Kontron Instruments, Inc., Everett, MA). The amount of MDA produced was monitored by measuring the increase of absorbance at 535 nm.

5.9 Degradation of rhodamine B

The amount of TiO_2 powders corresponding to 0.105 m^2 of exposed surface area was suspended in 2 mL of a 0.021 mM solution of rhodamine B. The suspension was transferred in a quartz vials, stirred in the dark for 30 minutes, and then irradiated for 90 minutes. 300 μL of the suspension were withdraw each 10 minutes, filtered through a 0.22 μm cellulose acetate filter and diluted 1:3 with water. The UV/vis spectra were measured by means of a UV/Vis spectrophotometer (Uvikon, Kontron Instruments, Inc., Everett, MA). The amount of rhodamine B consumed was evaluated by measuring the decrease of absorbance at 555 nm.

5.10 Generation of free radicals and singlet oxygen

The generation of radical species was monitored by electron spin resonance (EPR) spectroscopy (Miniscope 100 EPR spectometer, Magnettech, Berlin, Germany).

Instrument settings: microwave power 7 mW, modulation amplitude 1G, scan time 80s, two scans. The negative controls were, in all experiments, the solutions illuminated in the same conditions as the samples.

5.10.1 Superoxide radicals An amount of powder corresponding to an exposed surface area of 1.4 m^2 was suspended in 0.8 mL of 20 mM PBN (N-tert-butyl-α-phenylnitrone, Sigma-Aldrich, St. Louis, MO) solution in cyclohexane, and the suspension constantly stirred under illumination in a quartz vial. The EPR spectra were recorded on a sample suspension (50 µL) withdrawn after 60 minutes.

5.10.2 Hydroxyl radicals An amount of powder corresponding to an exposed surface area of 1.4 m^2 was suspended in 1.25 mL of a buffer solution (100 mM potassium phosphate buffer pH 7.4) of DMPO (5,5-dimethyl-1-pyrroline-N-oxide, Enzo Life Sciences, Inc.) 35 mM and the suspension constantly stirred under illumination in a quartz vial. The EPR spectra were recorded on a sample suspension (50 mL) withdrawn after 60 minutes.

5.10.3 Reaction with sodium formate An amount of powder corresponding to an exposed surface area of 1.4 m^2 was suspended in 0.5 mL of a buffer solution (125 mM potassium phosphate buffer pH 7.4) containing DMPO (75 mM) and sodium formate (1 M), and the suspension constantly stirred under illumination in a quartz vial. The EPR spectra were recorded on a sample suspension (50 µL).

5.10.4 Reaction with TEMPONE-H An amount of powder corresponding to an exposed surface area of 1.4 m^2 was suspended in 2 mL of water or phosphate buffer containing TEMPONE-H (1-hydroxy-2,2,6,6-tetramethyl-4-oxo-piperidine, Enzo Life Sciences, Inc.) 50 µM, and the suspension constantly stirred under illumination in a quartz vial. The EPR spectra were recorded on a sample suspension (50 µL).

5.10.5 Singlet oxygen An amount of powder corresponding to an exposed surface area of 1.4 m^2 was suspended in 1 mL of a 50 mM solution of 4-oxo-TMP (2,2,6,6-tetramethyl-4-piperidone, Sigma- Aldrich) in cyclohexane or 2 mL of a 50 mM solution of 4-oxo-TMP in phosphate buffer, and the suspension constantly stirred under

illumination in a quartz vial. The EPR spectra were recorded on a sample suspension (50 µL).

5.10.6 Singlet oxygen using rubrene 8 mg of rubrene were dissolved in 100 ml of a solution of butanol (1.8 mM) and acetonitrile (16 M) and stirred for at least 4 hours. An amount of powder corresponding to an exposed surface area of 0.105 m^2 was suspended in 2.5 ml of the solution and the suspension constantly stirred under illumination in a quartz vial. The TiO_2 samples were separated by centrifugation for 10 minutes. The supernatant was then filtrated with PTFE filter membranes (porosity 200 nm). The oxidation of rubrene was monitored by means of a UV/Vis spectrophotometer (Uvikon, Kontron Instruments, Inc., Everett, MA), evaluating the decrease of absorbance at 525 nm.

5.11 Simulation of EPR spectra The simulation of the spin trapping/EPR spectroscopy experimental signals were performed by using the software Winsim2002. (Winsim2002, version 0.98, National Institute of Environmental Health Science, National Institutes of Health, USA). The hyperfine splitting constants obtained from the optimisation of the simulation have been compared with those reported in the literature (NIESH S.T.B.D. database). The simulated spectra and the list of hyperfine splitting constants calculated in this work are reported in the SI.

Acknowledgements

This project has received funding from the European Union, Seventh Programme for research, technological development and demonstration under the project "Shape-engineered TiO_2 nanoparticles for metrology of functional properties: setting design rules from material synthesis to nanostructured devices " (SETNanoMetro), grant agreement No 604577.

The Authors are grateful to Dr. Paola Manetti, for her help in performing the experiments.

References

1. F. Piccinno, F. Gottschalk, S. Seeger and B. Nowack, *Journal of Nanoparticle Research*, 2012, **14**, 1-11.
2. OECD, ENV/JM/MONO(2011)53

3. REGULATION (EC) No 1223/2009
4. N. Serpone, D. Dondi and A. Albini, *Inorganica Chimica Acta*, 2007, **360**, 794-802.
5. A. G. Agrios and P. Pichat, *Journal of Applied Electrochemistry*, 2005, **35**, 655-663.
6. S. Ortelli, M. Blosi, C. Delpivo, D. Gardini, M. Dondi, I. Gualandi, D. Tonelli, V. Aina, I. Fenoglio, A. A. Gandhi, S. A. M. Tofail and A. L. Costa, *Journal of Photochemistry and Photobiology a-Chemistry*, 2014, **292**, 26-33.
7. H. Zhang, Y. Shan and L. Dong, *Journal of Biomedical Nanotechnology*, 2014, **10**, 1450-1457.
8. L. Visai, L. De Nardo, C. Punta, L. Melone, A. Cigada, M. Imbriani and C. R. Arciola, *International Journal of Artificial Organs*, 2011, **34**, 929-946.
9. M. Chiesa, M. C. Paganini, S. Livraghi and E. Giamello, *Physical Chemistry Chemical Physics*, 2013, **15**, 9435-9447.
10. T. Daimon, T. Hirakawa, M. Kitazawa, J. Suetake and Y. Nosaka, *Applied Catalysis a-General*, 2008, **340**, 169-175.
11. A. Lipovsky, L. Levitski, Z. Tzitrinovich, A. Gedanken and R. Lubart, *Photochemistry and Photobiology*, 2012, **88**, 14-20.
12. J. Cheng, E. Flahaut and S. H. Cheng, *Environmental Toxicology and Chemistry*, 2007, **26**.
13. A. Fujishima, X. Zhang and D. A. Tryk, *Surface Science Reports*, 2008, **63**, 515-582.
14. A. Carretero-Genevrier, C. Boissiere, L. Nicole and D. Grosso, *Journal of the American Chemical Society*, 2012, **134**, 10761-10764.
15. D. C. Hurum, A. G. Agrios, K. A. Gray, T. Rajh and M. C. Thurnauer, *Journal of Physical Chemistry B*, 2003, **107**, 4545-4549.
16. D. Del Rio, A. J. Stewart, N. Pellegrini, *Nutrition, Metabolism and Cardiovascular diseases*,2005, **15**, 316-328.
17. J. C. Zhao, T. X. Wu, K. Q. Wu, K. Oikawa, H. Hidaka and N. Serpone, *Environmental Science & Technology*, 1998, **32**, 2394-2400.
18. F. A. Villamena, C. M. Hadad and J. L. Zweier, *Journal of Physical Chemistry A*, 2003, **107**, 4407-4414.
19. S. Goldstein, A. Samuni and G. Merenyi, *Chemical Research in Toxicology*, 2004, **17**, 250-257.
20. E. Finkelstein, G. M. Rosen and E. J. Rauckman, *Molecular pharmacology*, 1982, **21**, 262-265.

21. P. Bilski, K. Reszka, M. Bilska and C. F. Chignell, *Journal of the American Chemical Society*, 1996, **118**, 1330-1338.
22. V. Brezova, S. Gabcova, D. Dvoranova and A. Stasko, *Journal of Photochemistry and Photobiology B-Biology*, 2005, **79**, 121-134.
23. I. Fenoglio, G. Greco, S. Livraghi and B. Fubini, *Chemistry-a European Journal*, 2009, **15**, 4614-4621.
24. D. Dvoranova, Z. Barbierikova and V. Brezova, *Molecules*, 2014, **19**, 17279-17304.
25. V. Roubaud, R. Lauricella, B. Tuccio, J. C. Bouteiller and P. Tordo, *Research on Chemical Intermediates*, 1996, **22**, 405-416.
26. H. Yokoyama, O. Itoh, M. Aoyama, H. Obara, H. Ohya and H. Kamada, *Magnetic Resonance Imaging*, 2000, **18**, 875-879.
27. A. Reis, M. R. M. Domingues, F. M. L. Amado, M. M. Oliveira and P. Domingues, *Free Radical Research*, 2008, **42**, 481-491.
28. S. Dikalov, M. Skatchkov, B. Fink and E. Bassenge, *Nitric Oxide-Biology and Chemistry*, 1997, **1**, 423-431.
29. S. I. Dikalov, M. P. Vitek, K. R. Maples and R. P. Mason, *Journal of Biological Chemistry*, 1999, **274**, 9392-9399.
30. K. P. Madden, *Radiation Research*, 1997, **147**, 335-341.
31. M. C. Krishna, A. Russo, J. B. Mitchell, S. Goldstein, H. Dafni and A. Samuni, *Journal of Biological Chemistry*, 1996, **271**, 26026-26031.
32. I. Fenoglio, J. Ponti, E. Alloa, M. Ghiazza, I. Corazzari, R. Capomaccio, D. Rembges, S. Oliaro-Bosso and F. Rossi, *Nanoscale*, 2013, **5**, 6567-6576.
33. J. I. Kim, J. H. Lee, D. S. Choi, B. M. Won, M. Y. Jung and J. Park, *Journal of Food Science*, 2009, **74**.
34. E. L. Clennan and A. Pace, *Tetrahedron*, 2005, **61**, 6665-6691.
35. C. Schweitzer and R. Schmidt, *Chemical Reviews*, 2003, **103**, 1685-1757.
36. E. Burello and A. P. Worth, *Nanotoxicology*, 2015, **9**, 116-117.
37. I. Fenoglio, B. Fubini, E. M. Ghibaudi and F. Turci, *Advanced Drug Delivery Reviews*, 2011, **63**, 1186-1209.
38. H. Ma, A. Brennan and S. A. Diamond, *Environmental Toxicology and Chemistry*, 2012, **31**, 1621-1629.
39. C. Takahashi, Y. Tsujimoto and Y. Yamamoto, *Journal of Clinical Biochemistry and Nutrition*, 2012, **51**, 128-131.

40. J. E. Biaglow, Y. Manevich, F. Uckun and K. D. Held, *Free Radical Biology and Medicine*, 1997, **22**, 1129-1138.
41. P. C. Dedon, *Chemical Research in Toxicology*, 2008, **21**, 206-219.
42. L. Zhang and J. M. Cole, *Acs Applied Materials & Interfaces*, 2015, **7**, 3427-3455.
43. L. Pan, J.-J. Zou, X.-Y. Liu, X.-J. Liu, S. Wang, X. Zhang and L. Wang, *Industrial & Engineering Chemistry Research*, 2012, **51**, 12782-12786.
44. D. C. Grinter, T. Woolcot, C.-L. Pang and G. Thornton, *Journal of Physical Chemistry Letters*, 2014, **5**, 4265-4269.
45. A. Marucco, F. Catalano, I. Fenoglio, F. Turci, G. Martra and B. Fubini, *Chemical Research in Toxicology*, 2015, **28**, 87-91.
46. W. Kudo, M. Yamato, K.-I. Yamada, Y. Kinoshita, T. Shiba, T. Watanabe and H. Utsumi, *Free Radical Research*, 2008, **42**, 505-512.
47. K. Hashimoto, H. Irie and A. Fujishima, *Japanese Journal of Applied Physics Part 1-Regular Papers Brief Communications & Review Papers*, 2005, **44**, 8269-8285.
48. T. Ohno, K. Sarukawa, K. Tokieda and M. Matsumura, *Journal of Catalysis*, 2001, **203**, 82-86.
49. C. Deiana, M. Minella, G. Tabacchi, V. Maurino, E. Fois and G. Martra, *Physical Chemistry Chemical Physics*, 2013, **15**, 307-315.
50. J. R. Gurr, A. S. S. Wang, C. H. Chen and K. Y. Jan, *Toxicology*, 2005, **213**, 66-73.
51. C. Xue, J. Wu, F. Lan, W. Liu, X. Yang, F. Zeng and H. Xu, *Journal of Nanoscience and Nanotechnology*, 2010, **10**, 8500-8507.
52. K. Gerloff, I. Fenoglio, E. Carella, J. Kolling, C. Albrecht, A. W. Boots, I. Foerster and R. P. F. Schins, *Chemical Research in Toxicology*, 2012, **25**.
53. C. M. Sayes, R. Wahi, P. A. Kurian, Y. P. Liu, J. L. West, K. D. Ausman, D. B. Warheit and V. L. Colvin, *Toxicological Sciences*, 2006, **92**, 174-185.
54. V. Bolis, C. Busco, M. Ciarletta, C. Distasi, J. Erriquez, I. Fenoglio, S. Livraghi and S. Morel, *Journal of colloid and interface science*, 2012, **369**, 28-39.
55. J. Erriquez, V. Bolis, S. Morel, I. Fenoglio, B. Fubini, P. Quagliotto and C. Distasi, *Nanomedicine : nanotechnology, biology, and medicine*, 2015, **11**, 1309-1319.

Table 1. Physico-chemical properties of the TiO_2 nanopowders

	Elemental analysis (w/w%)[a]	Crystalline phase[b]	Specific surface area (m^2/g)	Crystallite size (nm)[b]	ζ potential (water, pH 7.4)
T-A	TiO_2 99.6; Fe_2O_3 0.08; Al_2O_3 0.19; SiO_2 0.11	100% anatase	54.3	18 ± 4.4	-37.1
T-A/R	TiO_2 99.6; Fe_2O_3 0.08; Al_2O_3 0.02; SiO_2 0.12	85% anatase 15% rutile	23.5	49.5 ± 7.7	-41.4
T-A/R P25	TiO_2 99.6; Fe_2O_3 0.08; Al_2O_3 0.18; SiO_2 0.12	77% anatase 23% rutile	52.6	26.8 ± 4.3	-21.5
T-R1	TiO_2 99.5; Fe_2O_3 0.12; Al_2O_3 0.15; SiO_2 0.12	100% rutile	39.1	46.6 ± 3.5	-38.5
T-R2	TiO_2 93.8; MnO_2 0.03; Al_2O_3 4.67; SiO_2 1.42	100% rutile	44.8	77.9 ± 7.3	-40.5

[a] XRF, this work except for R2 (data declared by the company); [b] XRD

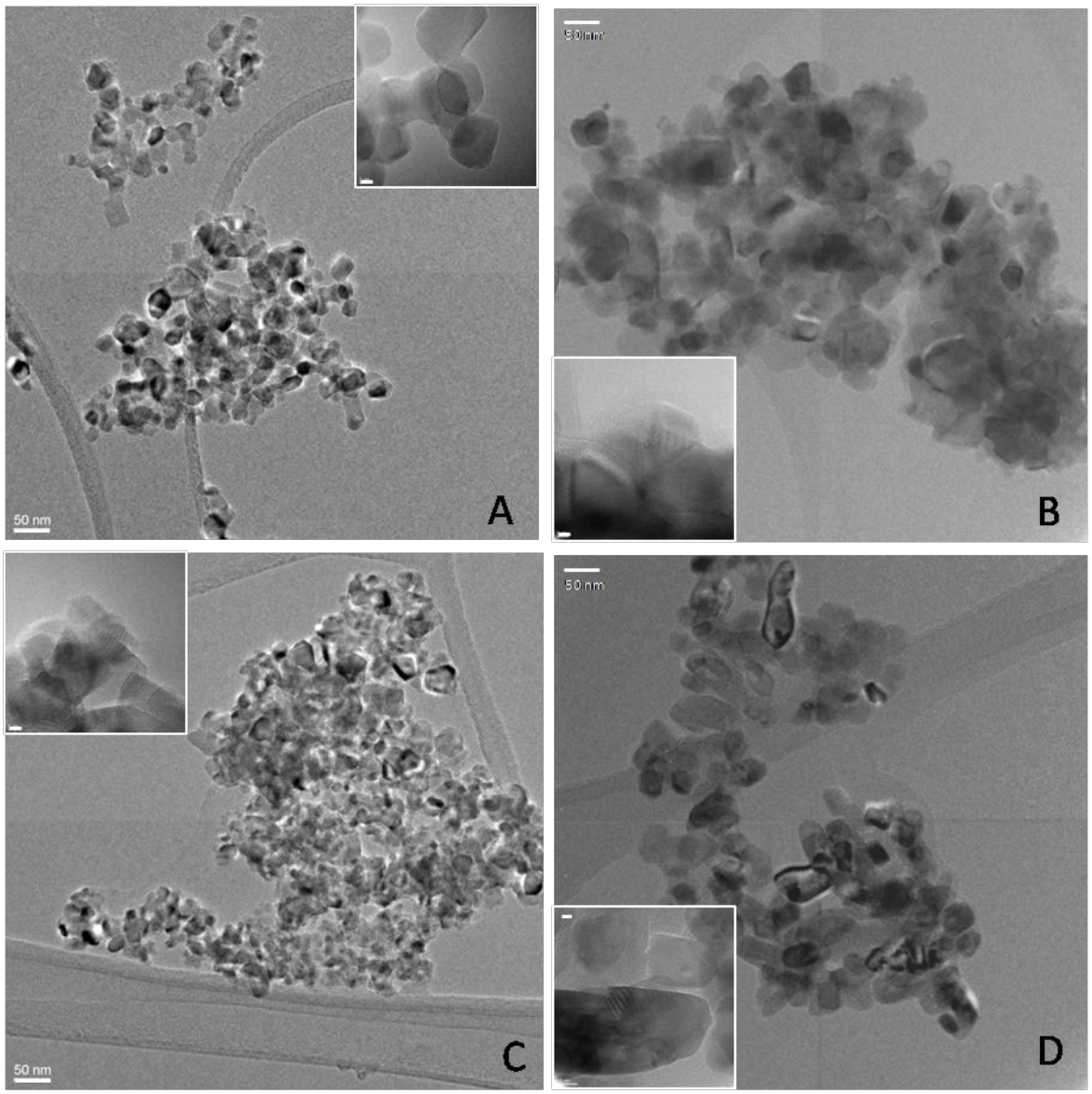

Figure 1. TEM micrographs of A) T-A/R P25; B) T-A/R; C) T-A; D) T-R1. In the insets images at higher magnification (bars = 5 nm) are shown.

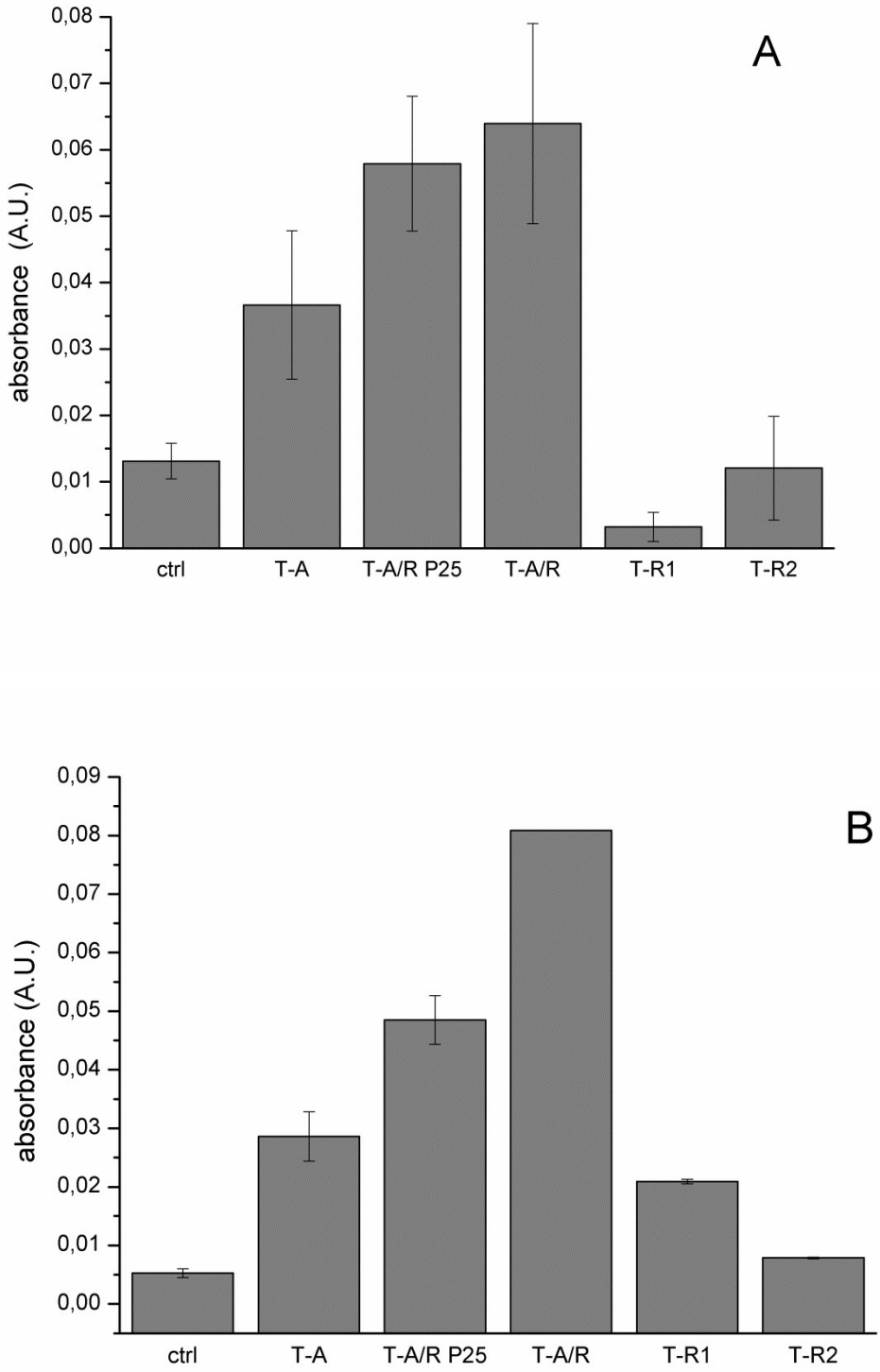

Figure 2. Degradation of A) linoleic acid and B) 2-deoxyribose. The extent of degradation is evaluated by measuring the amount of MDA generated. The data are express as means ± SD obtained in three independent experiments

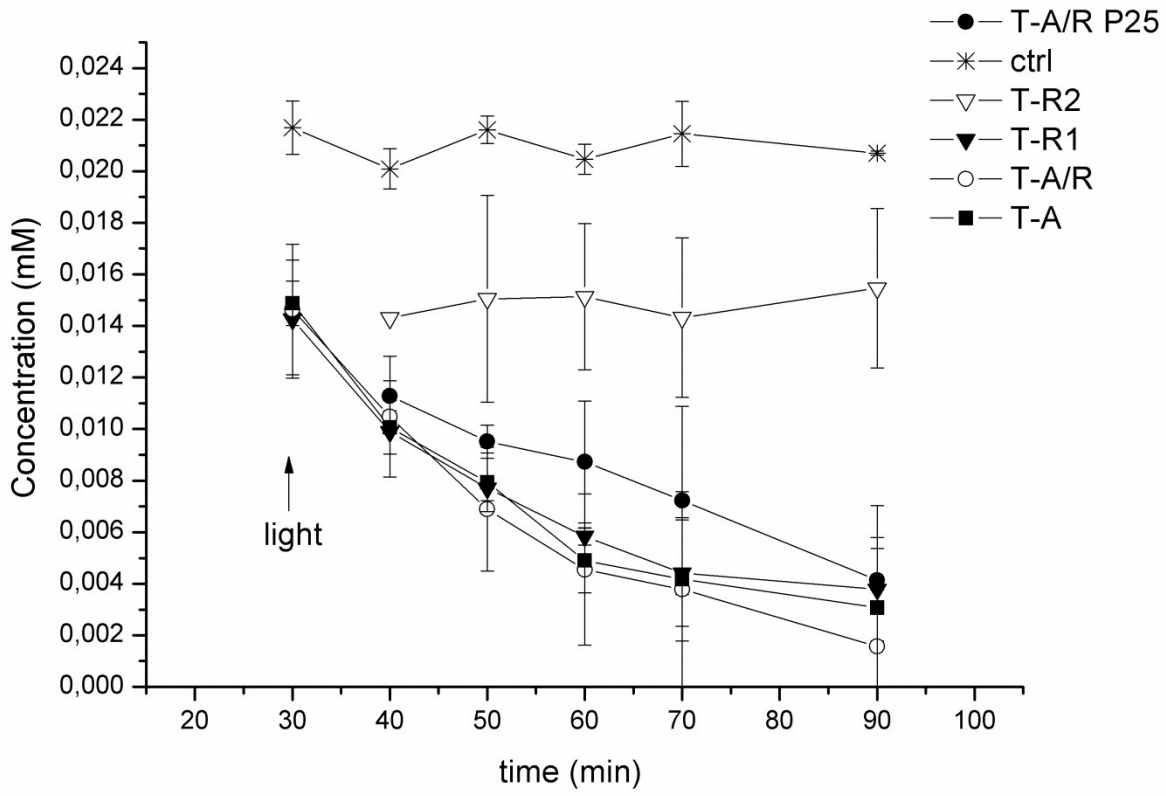

Figure 3. Degradation of rhodamine B. Data are express as means ± SD obtained in three independent experiments

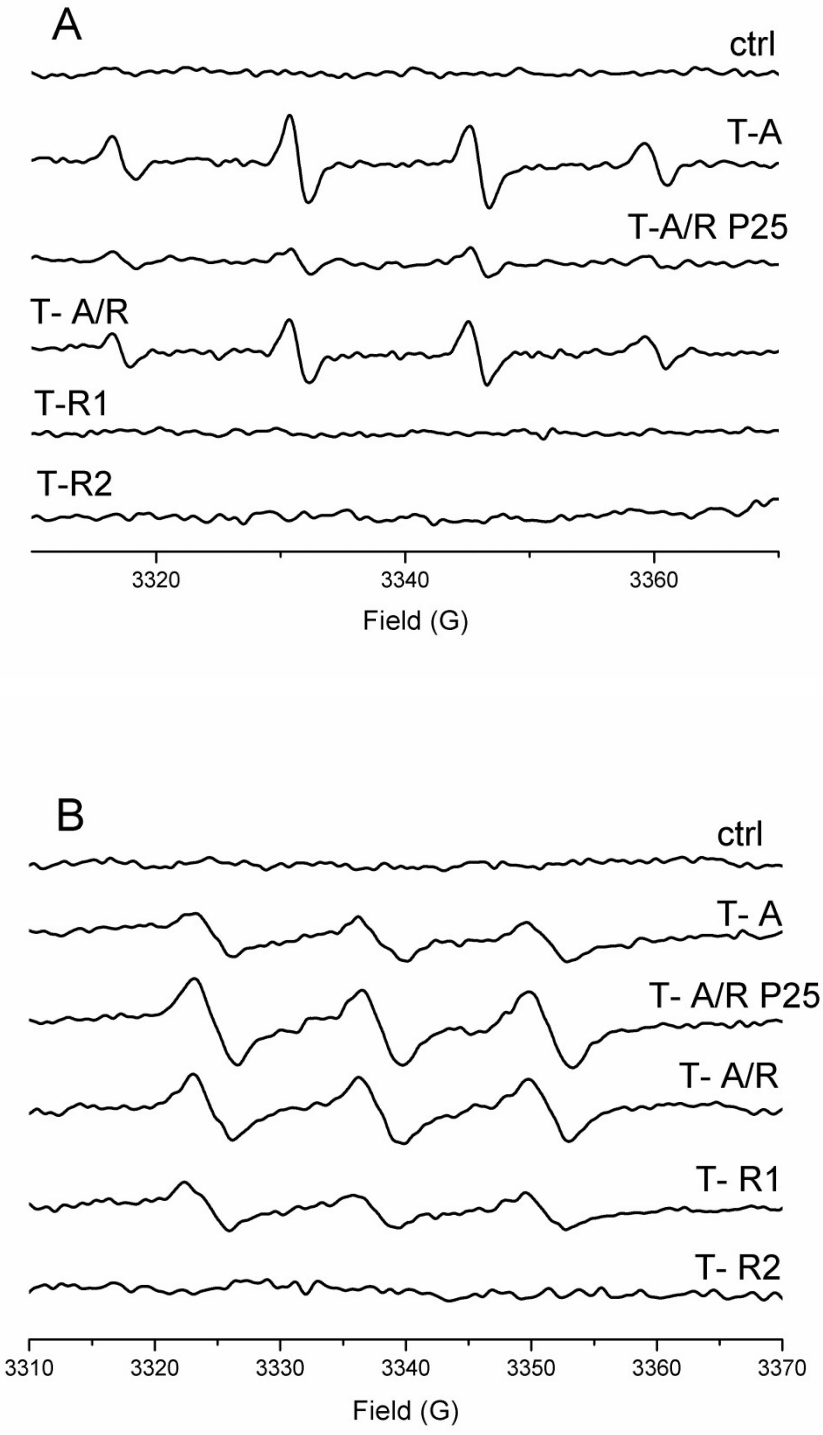

Figure 4. Generation of (A) hydroxyl radicals (phosphate buffer pH 7.4, DMPO) and (B) superoxide anions radicals (cyclohexane, PBN) by the TiO_2 samples. The representative EPR spectra, recorded after 60 minutes of irradiation, corresponds (see SI) to the adduct DMPO/$HO^{\cdot}$ in (A) and PBN/$O_2^{-\cdot}$ (B). The amount of radicals are proportional to the intensity of the signal.

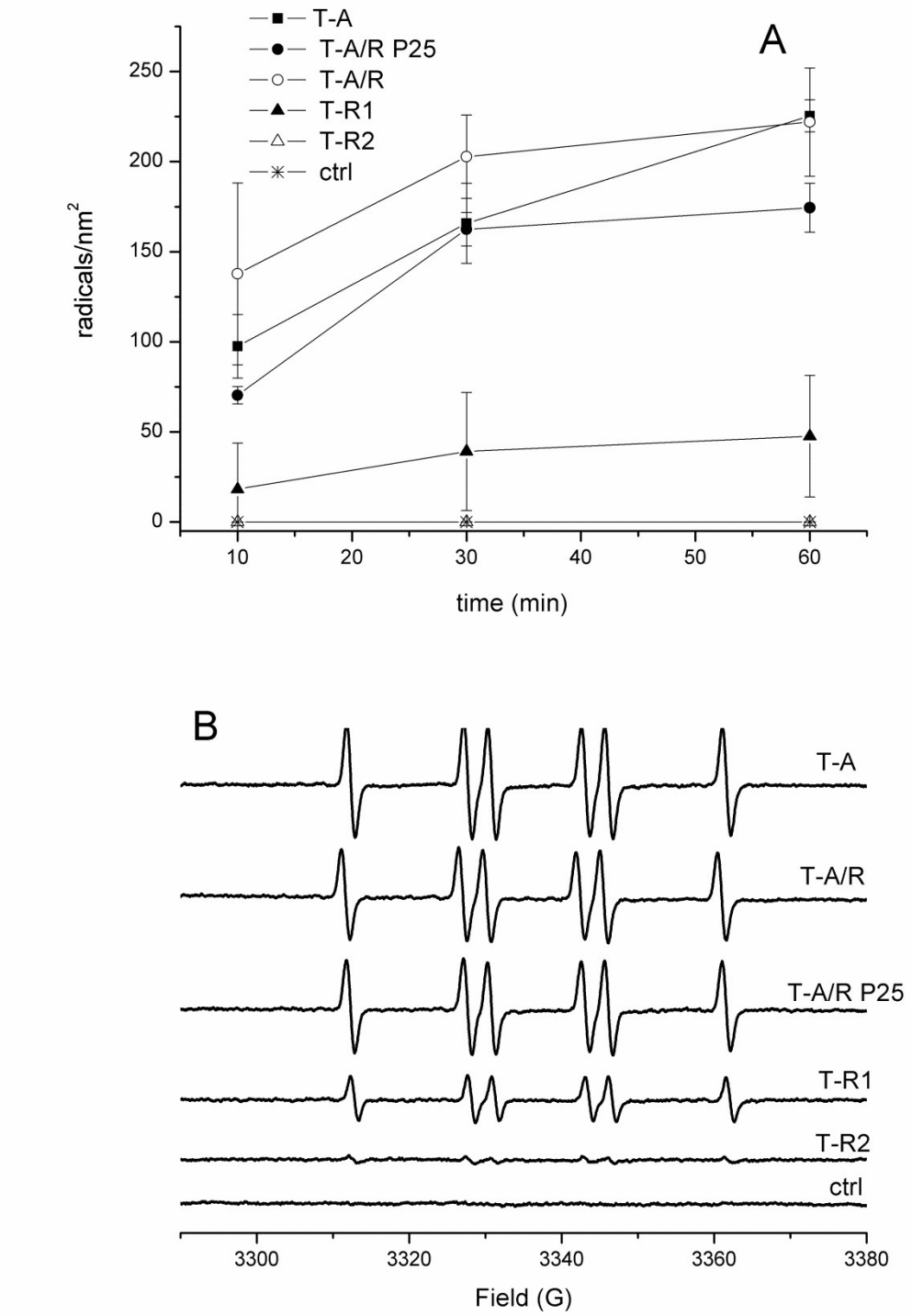

Figure 5. Generation of carboxylate radicals by the TiO_2 samples in contact with a solution (phosphate buffer pH 7.4, DMPO) of sodium formate. A) Amount of carboxylate radicals generated during the time of irradiation expressed as amount of radicals generated per unit surface area of the powder; B) representative spectra recorded after 60 minutes of irradiation. The EPR spectra corresponds (see SI) to the adduct DMPO/$CO_2^{-\cdot}$.

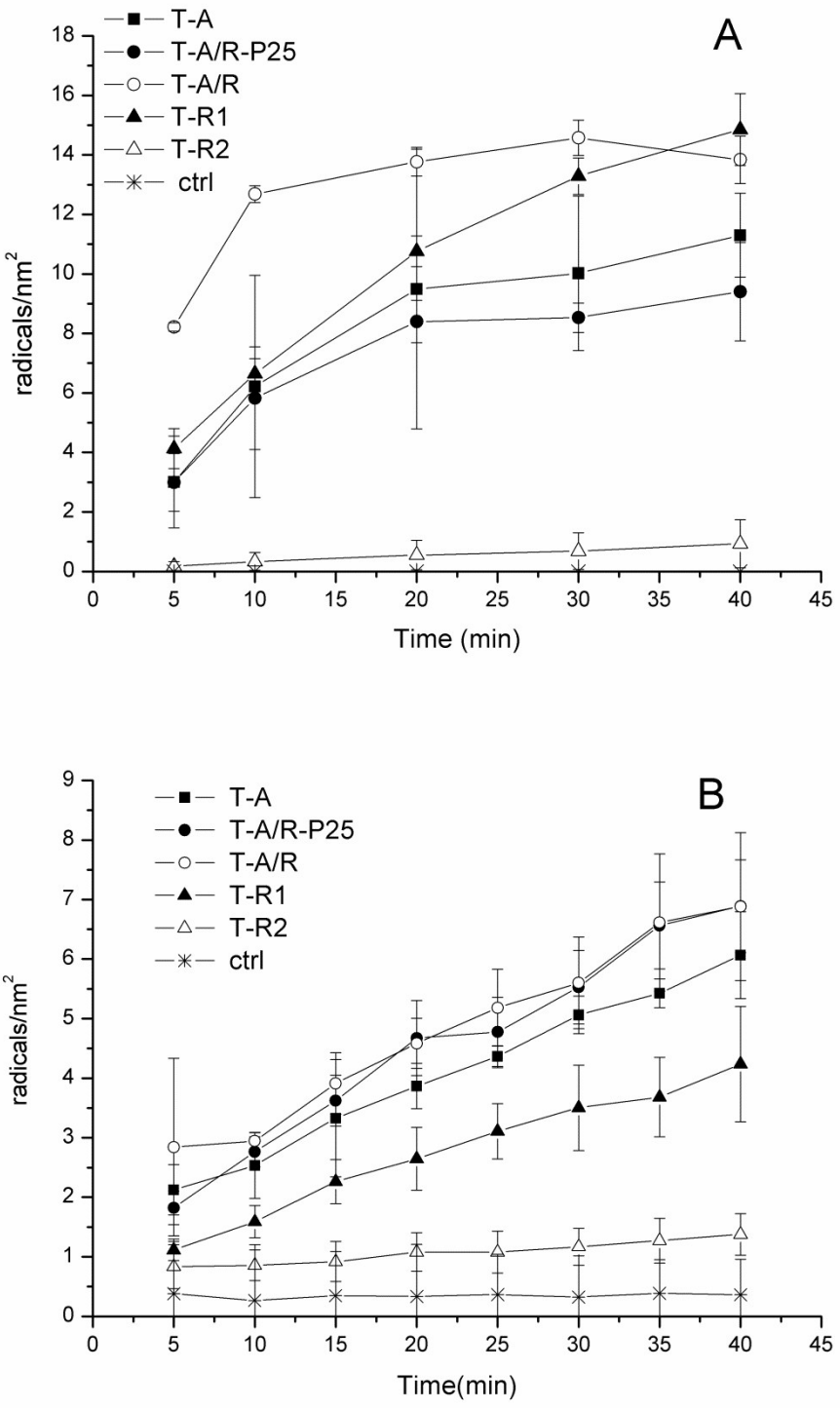

Figure 6. Generation of TEMPONE radical by the TiO_2 samples in contact with a solution of TEMPONE-H: A) in water; B) in phosphate buffer, pH 7.4. The data are expressed as amount of radicals generated per unit surface area of the powder.

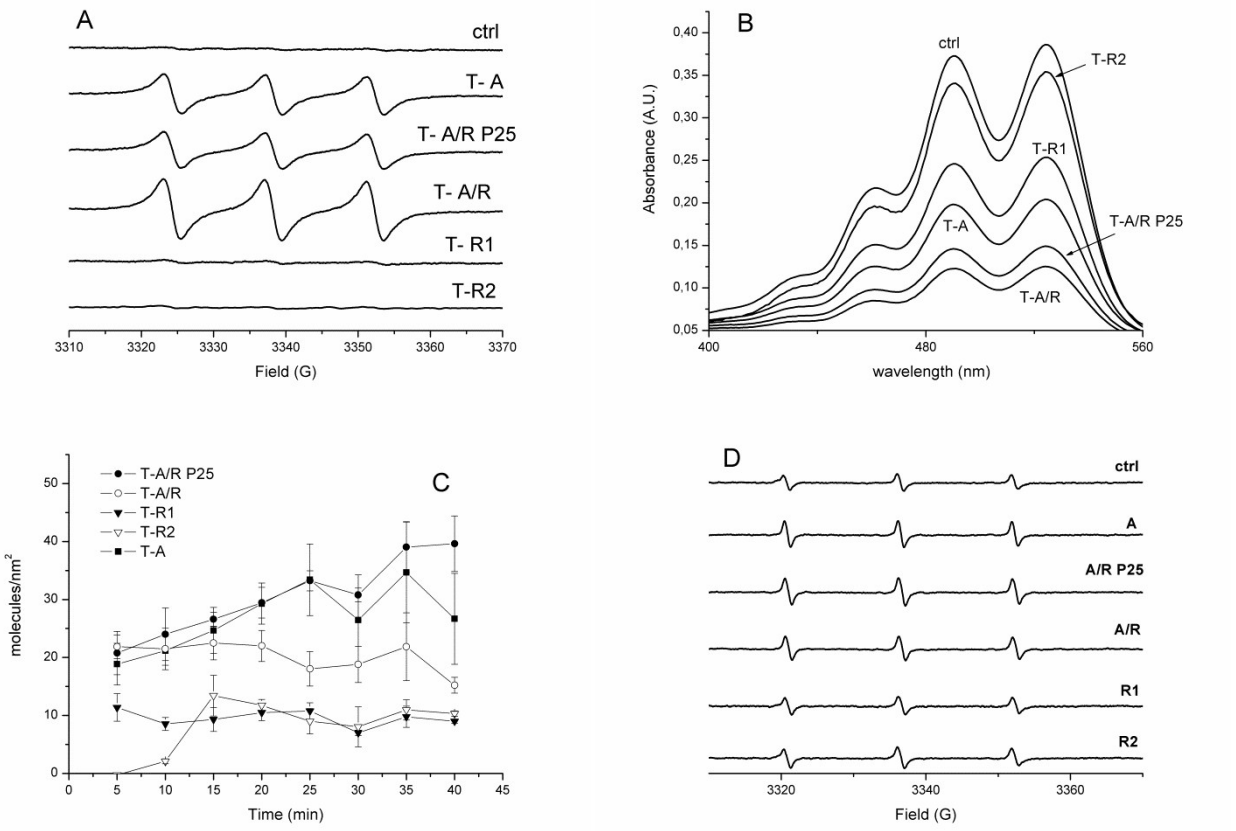

Figure 7. Generation of singlet oxygen by the TiO_2 samples. (A) representative spectra after 40 minutes of irradiation generated in a solution of 4-oxo-TMP in cycloexane. (B) UV/vis spectra showing the oxidation of rubrene by photo-generated singlet oxygen; (C) amount of TEMPONE radical generated in a solution of 4-oxo-TMP in phosphate buffer; (D) representative spectra after 40 minutes of irradiation.